TOPOGRAPHIC ROUGHNESS PROFILES ACROSS IMPACT CRATERS ON ASTEROID (101955) BENNU FROM THE OSIRIS-REx LASER ALTIMETER. F. M. Rossmann[1], C. L. Johnson[1], E. B. Bierhaus[2], M. Al Asad[3], O. S. Barnouin[4], R. T. Daly[4], M. G. Daly[5], J. Seabrook[5]. [1]Department of Earth, Ocean and Atmospheric Sciences, University of British Columbia, Vancouver, Canada, [2]Lockheed Martin Space, Littleton, CO, USA, [3]University of California, Berkeley, California, [4]Johns Hopkins University Applied Physics Laboratory, Laurel, MD, [5]Centre for Research in Earth and Space Science, York University, Toronto, Ontario, Canada.

Introduction: Images and lidar data of the surface of asteroid (101955) Bennu from the OSIRIS-REx Camera Suite (OCAMS) [1] and the OSIRIS-REx Laser Altimeter (OLA) [2] have revealed the presence of at least 400 craters with diameters 5 – 80 m over the asteroid's surface [3]. To date, investigations of Bennu's craters have focused on their spatial distributions and global size-frequency distributions [4, 5] crater depth-to-diameter ratios [6], color [7] and their potential to probe sub-surface structure [8]. Furthermore, OCAMS images show that the particle size-frequency distribution of granular material in impact craters is heterogenous among craters [8] reflecting the net result of the excavation of target material during an impact, and the subsequent degradation of crater morphology. Here, we analyze topographic variability (roughness) on spatial scales of 50 – 200 cm using data from on the OSIRIS-REx mission. Specifically, we construct radially-averaged profiles of topographic variability for a population of 423 impact craters over the asteroid's surface, and use Principal Component Analysis (PCA) to investigate dominant modes of radial variations in roughness.

Data and Methods: We used OLA (Science Level 2A) point clouds from the Orbital B phase of the mission [9], produced by the OSIRIS-REx Altimetry Working Group. These point clouds (and the spacecraft positions) have been globally registered to minimize differences among overlapping, individual OLA scans [10]. The average spatial data density is ~500 pts / m^2 and the OLA spot size during Orbital B phase was ~5 cm diameter [9]. We analyzed topographic variability for 423 craters with diameters 5–80 m [3]. The minimum crater diameter was limited to 5 m, to ensure that radial roughness profiles could be constructed at a range of baselines. The maximum crater diameter was set to 80 m so that the crater and its surrounding region (out to 3 crater radii) did not cover more than ~1/16 of Bennu areally. The crater population has global coverage.

We first combined and downsampled the L2A data onto a 10 cm point cloud to produce a data set with a more uniform spatial data density that was also more manageable in size. We then established nodes corresponding to the locations of the data set downsampled to 25 cm. For each node, a kd-tree neighbour-in-radius search was implemented on the 10 cm point cloud. Neighbours within a specified baseline distance (B) of the node were binned and detrended with a best-fitting plane estimated using orthogonal distance regression. The mean position of the binned points and the variability (standard deviation) of orthogonal heights above the regression plane were calculated. The standard deviation of the detrended points in each bin is a measure of the local variability in geometric height (*i.e.*, the roughness metric, ξ of [11]) at a given baseline distance. The procedure was repeated for choices of B = 50, 100, 150 and 200 cm. We initially also attempted the calculations for B = 25 cm but found that at these shorter baselines any residual mismatch of the scans in the L2A data affected the results, even after attempting an additional local registration step. An example is shown for Osprey crater, a 21-m diameter crater

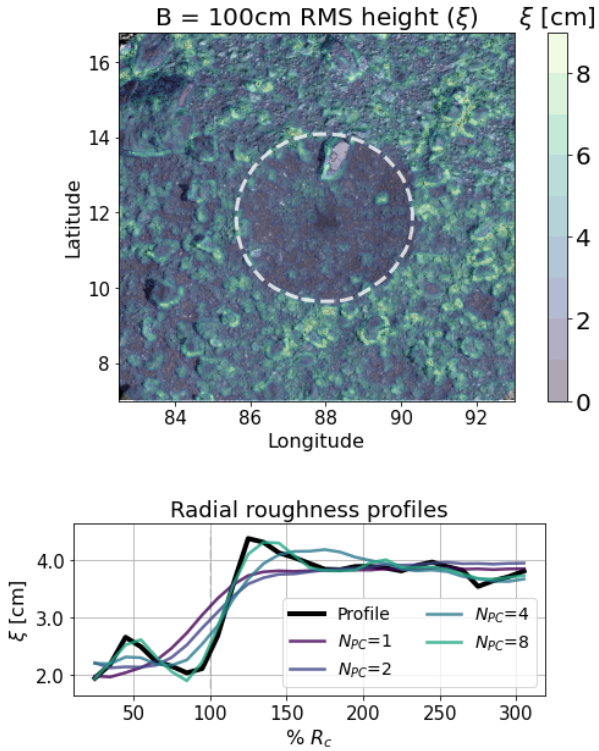

Figure 1: (a) OCAMS mosaic [12] of TAG candidate site Osprey overlain by 100 cm baseline roughness (color bar). (b) Radial roughness profile (black line) for Osprey extending to three crater radii, R_C, superposed with reconstructed roughness profiles using 1, 2, 4 and 8 principal component (PC) modes.

centered at (11.7 °N, 87.9 °E) for B = 100 cm (Figure 1a). For each crater, we produced radially averaged roughness profiles from the crater center (Figure 1b) to 300% of the crater radius in 10% increments.

We used PCA to investigate any characteristic radial variations in roughness for Bennu's craters. The PCA data matrix is formed by stacking zero-centered roughness profiles together to form a 423x30 matrix, and each column of the matrix is centered by removing its mean value (equivalent to removing the 'average' roughness profile). The PCA is implemented through singular value decomposition of the data matrix.

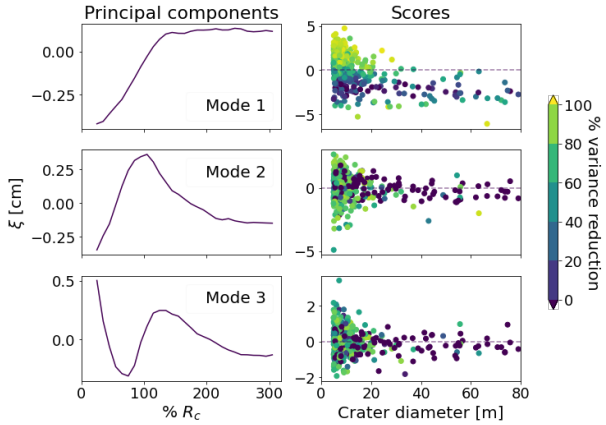

Figure 2: First three principal component modes and their corresponding scores. These modes account for 77% of the total variance in the dataset. The scores (i.e., the weight attributed to each mode for an individual crater) are variable at small crater diameters and relatively constant at larger crater diameters. Scores are coloured by the percentage of the variance of the original roughness profile for an individual crater that is accounted for by each mode.

Results and Discussion: The first principal component (PC1) accounts for 53.3% of the variance in the dataset and describes a transition in roughness from the crater interior to just beyond the edge of the crater (~120% R_C). Beyond the crater rim, PC1 is relatively constant to ~300 R_C. The smooth shape of PC1 is very similar to the average roughness profile of the sample crater population. Typically, positive PC1 scores (the contribution of each mode to an individual profile) correspond to craters less than about 25 m in diameter, indicating an increasing roughness from the crater center outwards for this subset of the overall crater population. The second principal component (PC2) has local maximum located roughly at the crater rim and accounts for about 16.0% of the total variance in the dataset. This mode can sharpen (or not, depending on the sign of the score) the transition from interior to exterior roughness for a given crater. The third principal component (PC3) describes 7.7% of the total variance in the dataset. The distribution of PC2 and PC3 scores occupies both positive and negative values but tends to be largest in amplitude for small craters. All three modes also have low amplitude, generally negative coefficients at large crater diameters, suggesting overall less difference in interior and exterior roughness.

Roughness profiles can be reconstructed for a specified number of PCs, adding the result to the average profile. Variance reduction for individual and combined PCA modes can also be calculated for each crater. Variance reduction for the first mode is >80%, for ~65% of the population, especially for craters less than about 25 m in diameter. Poor variance reduction is still found across some craters of all sizes. Craters whose roughness profiles show high amplitude, positive PC1 scores, also show good variance reduction, reflecting relatively smooth crater interiors that increase in roughness towards a background value with increasing distance from the crater center. Overall, the results here suggest that a substantial population of craters, especially those with diameters less than ~25 m have lower interior roughness than their surroundings. This supports other work that suggests the presence of a fine-grained sub-surface layer on Bennu, evidenced in

crater morphologies [8]. However, a small percentage of craters with diameters less than 25m are similar to larger craters that have more muted interior/exterior roughness differences. As yet, there is no clear indication of e.g., geographical or other controls on this subset of the crater population, although this is still under investigation.

Acknowledgments: This work was enabled by the collaborative efforts of the OSIRIS-REx Team, supported by NASA under Contract NNM10AA11C issued through the New Frontiers Program. The OLA instrument build and Canadian science support were provided by contracts with the Canadian Space Agency.

References: [1] Rizk, B. et al. (2018). *SSR*, v. 214, 26. [2] Daly, M. G., et al. (2017). *SSR*, v. 212, 899–924. [3] Bierhaus, E. B. et al., (2022), in review *Nat. Geosci.* [4] Walsh K. J. et al. (2019) *Nat. Geosci., 12,* 242–246. [5] Ballouz R. et al. (2020) *Nature., 587,*s–209. [6] Daly R. T. (2020) *Geophys. Res. Lett. 47.* [7] DellaGiustina D. N. et al (2020) *Science,* 370. [8] Bierhaus E. B. et al. (2020), *LPSC MMXX,* Abstract #2156. [9] Daly, M. G. et al. (2020), *Sci. Adv.,* 6, eabd 3649. [10] Daly M. et al. (2020) UA-SIS-9.4.4-302, Rev. 5.0. [11] Shepherd, M. K et al. (2001), *JGR., 106*, 32,777–32,795. [12] Bennett, C. A., et al. (2021), *Icarus,* 357, 113690.